Numerical Solution of Three-Dimensional Shock Wave and Turbulent Boundary-Layer Interaction

C. M. Hung* and R. W. MacCormack†
NASA Ames Research Center, Moffett Field, Calif.

A newly developed, rapid numerical scheme is used to solve the complete mass-averaged Navier-Stokes equations for supersonic turbulent flow over a three-dimensional compression corner. A simple eddy viscosity model is developed, and the interaction of a swept shock wave and a three-dimensional turbulent boundary layer is studied. Good agreement is obtained between the present results and experimental measurements for the case of a wedge with angle $\alpha = 6$ deg on a flat-plate sidewall. For the case of $\alpha = 12$ deg, the computed results do not show the existence of a peak pressure found experimentally. However, the range of interaction, the plateau pressure, and the peak heat transfer are closely predicted for all cases. The high heat transfer near the axial corner is due to the thinning of the boundary layer and inflow of fresh high-momentum fluid. The heat transfer is relieved through pressure reduction and boundary-layer thickening.

Nomenclature

C_H = local heat-transfer coefficient (Stanton number)
$C_{H\infty}$ = local undisturbed heat-transfer coefficient
c_p = specific heat at constant pressure
D = van Drist damping factor, Eq. (2)
d = "modified distance," Eq. (5)
E = total energy
JL = number of mesh points in the y direction
$JLFM$ = number of fine mesh points in the y direction
KL = number of mesh points in the z direction
$KLFM$ = number of fine mesh points in the z direction
L = characteristic length from flat-plate leading edge to wedge
Lx, Ly, Lz = split finite-difference operators in the x, y, and z directions, respectively
Lyh, Lzh = hyperbolic difference operators in the y and z directions
Lyp, Lzp = parabolic difference operators in the y and z directions
ℓ = mixing length, Eq. (4)
M_∞ = freestream Mach number
Pr_t = turbulent Prandtl number, 0.9
p = averaged static pressure, $p = \rho RT$
p_∞ = averaged freestream static pressure
R = gas constant
Re_L = Reynolds number based on characteristic length L
T = absolute static temperature, °R
T_∞ = freestream temperature
T_w = wall temperature
t = time
Δt = time increment
U = conservative flow variables (ρ, ρu, ρv, ρw, E)
u_∞ = freestream velocity
u, v, w = velocity components in the Cartesian (x,y,z) coordinates
x_0 = upstream boundary location
x_w = coordinate along wedge surface
x, y, z = Cartesian coordinates
y_f, z_f = dimensions of fine mesh in the $(y\text{-}z)$ plane
y_h, z_h = dimensions of the $(y\text{-}z)$ plane computation domain
y_s = inviscid shock distance in the y direction, from wedge surface
$\Delta y)_{\min}, \Delta z)_{\min}$ = minimum mesh spacings in the y and z directions
α = wedge angle
γ = ratio of specific heat, 1.4
δ = value of d, Eq. (5), at the edge of boundary layer
ϵ = turbulent eddy viscosity, Eq. (1)
λ = length scale constant, 0.08
μ_w = molecular viscosity at the wall
ρ = averaged specific density
ρ_w = specific density at the wall
τ_w = shear stress at the wall
ω = absolute value of vorticity, Eq. (3)

Presented as Paper 78-161 at the AIAA 16th Aerospace Sciences Meeting, Huntsville, Ala., Jan. 16-18, 1978; submitted Feb. 21, 1978; revision received July 5, 1978.

Index categories: Boundary Layers and Convective Heat Transfer—Turbulent; Computational Methods; Supersonic and Hypersonic Flow.

*Research Scientist. Member AIAA.
†Assistant Chief, Computational Fluid Dynamics Branch. Member AIAA.

Introduction

TWO-DIMENSIONAL shock wave boundary-layer interactions have been studied extensively, and the flow mechanism, as well as the interaction features, are now quite well known and can be simulated numerically fairly well. However, in actual design, most of the interaction flows are three-dimensional in character and very often incorporate strong gradients of flow properties in each of the three space dimensions. As a result, the flowfield features and the governing equations are complex and have received only a few experimental and theoretical investigations.

One of the three-dimensional interaction problems that has attracted a substantial amount of interest (e.g., Refs. 1-6) is the problem of supersonic flow over an axial corner where the shock wave generated by one compression surface sweeps across the boundary layer of a second flat surface (Fig. 1). One obvious reason for the interest is the simplicity of its geometry. Very often experimentalists have placed just a wedge in the wind tunnel and used one of the tunnel walls as the second flat surface. Another reason, perhaps the most important one, is that this geometry indeed occurs in many configurations of practical importance such as in airbreathing engine inlets, at wing-body junctures, and at the intersection of several supersonic control surfaces. Experimental

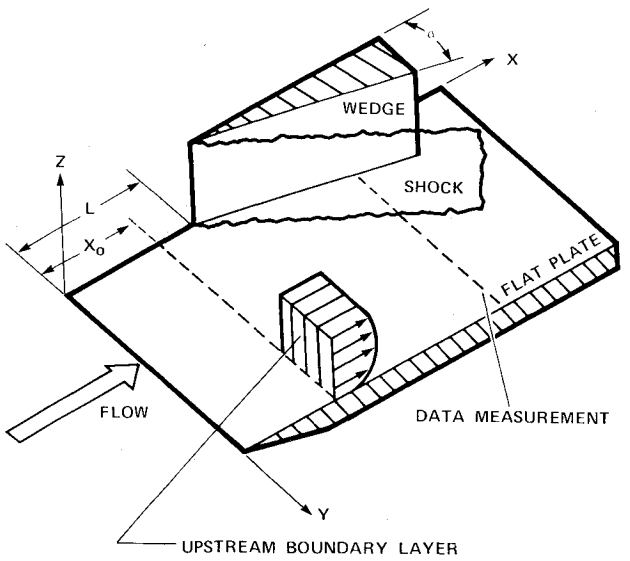

Fig. 1 Three-dimensional compression corner and swept shock wave.

measurements[6] have shown that the three-dimensional interactions can produce local surface heat-transfer rates on the flat surface, near the axial region, that are greater by a factor of about 2 than those produced by the corresponding two-dimensional interactions, compared on the basis of an equal overall surface pressure rise.

Inviscid calculations for a similar geometry, with two intersecting wedges and various swept leading-edge angles, have been obtained in a similarity coordinate system by Kutler[7] and by Shanker et al.[8] Shang and Hankey[9] numerically solved the Navier-Stokes equations for a three-dimensional hypersonic corner flow. They first used an explicit finite-difference scheme[10] to solve laminar flow problems in a conical coordinate system. It took about 10 h CPU time on a CDC 7600 for a converged solution with $8\times32\times36$ mesh points. Later, Shang[11] used an implicit scheme in the inner fine mesh region, and the computation time was reduced by a factor of about 10.

Hung and MacCormack[12] extended a rapid numerical scheme[13] to three dimensions to solve the complete Navier-Stokes equations for a supersonic flow over a compression corner with sidewall effects. The program first was verified for laminar flow cases. With a total mesh of $30\times30\times30$, it took about 1.2 h CPU time on a CDC 7600 for a converged solution. Moreover, the numerical scheme is nearly independent of Reynolds number, and hence, in the present study, it is extended to high Reynolds number turbulent flow.

The objectives of the present investigation are to demonstrate the feasibility of numerically solving supersonic turbulent flows over a three-dimensional compression corner and to study the associated three-dimensional shock wave boundary-layer interactions. The mass-averaged three-dimensional Navier-Stokes equations with an eddy viscosity model are utilized to fully describe the inviscid-viscous interactions. The use of the full Navier-Stokes equations by no means implies that every term in the equations is properly resolved everywhere. The flowfield is calculated as a whole with the same set of equations, thus avoiding the need to match solutions from different flow regions. A turbulence model developed by Baldwin and Lomax[14] also is modified and tested for the present three-dimensional corner flow calculations. The experiments conducted by Law[15] are selected for comparison at Mach number 5.9 and unit Reynolds number of 0.3281×10^6/cm with wedge angles of 6 and 12 deg. Detailed viscous and inviscid interaction features will be presented in the form of pressure and heat-transfer distributions on the flat surfaces and the static pressure on (y-z) planes. The mechanism of causing high heat transfer near the axial corner will be discussed.

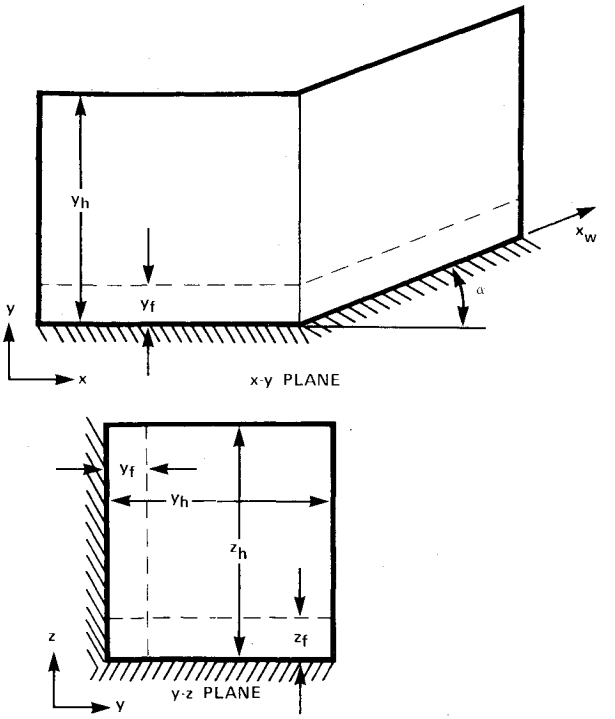

Fig. 2 Cross-sectional views of the computational domain.

Analysis

Numerical Procedure

Figure 2 shows cross sections of the computational domain in the (x-y) and (y-z) planes. The mesh is spaced equally in the x direction, but, in both y and z directions, a fine mesh spacing is used in the regions near the wall, $0<y\le y_f$ and $0\le z\le z_f$, to resolve the viscous regions, and a coarse mesh spacing is used in the outer regions, $y_f\le y\le y_h$ and $z_f\le z\le z_h$, where viscous effects are negligible. Both the fine and coarse meshes are stretched geometrically with different stretching constants.

The governing equations of the present analysis are the time-dependent, compressible Navier-Stokes equations, casted in terms of mass-averaged variables, with the bulk viscosity and the specific turbulent energy in the normal stress components omitted. The resulting mean conservative relations are the same as their laminar flow counterpart, except for the addition of the Reynolds stress tensor and the Reynolds heat flux. Turbulent closure is accomplished by expressing the Reynolds stress tensor in terms of the product of an eddy viscosity ϵ with the mean velocity gradients. Also, a turbulent Prandtl number Pr_t is used for the Reynolds heat flux. The equations then are split into three groups corresponding to the coordinate directions for treatment by three operators: Lx, Ly, Lz. A conventional explicit two-step numerical scheme[10] is used in the Lx operator and in the Ly and Lz operators for the outer coarse mesh regions:

$$Lx(0-y_h,\quad 0-z_h)$$

$$Ly(y_f-y_h,\quad 0-z_h)$$

$$Lz(0-y_h,\quad z_f-z_h)$$

where the arguments inside the parentheses indicate the regions in which the operators are applied. In the inner regions, the Ly and Lz operators are split further into

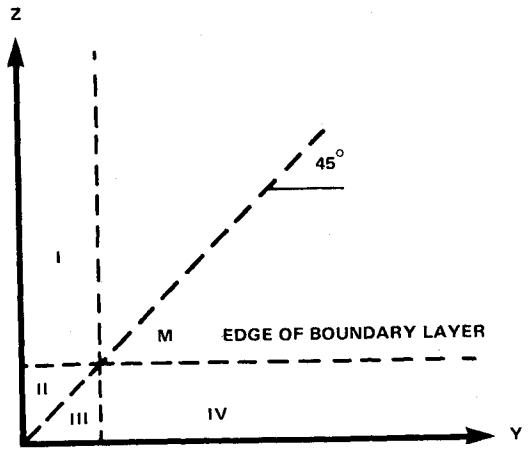

Fig. 3 Division of four viscous regions in (y-z) plane.

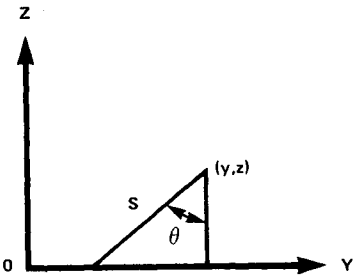

Fig. 4 Sketch of integration formula.

hyperbolic and parabolic operators for the inviscid (Lyh and Lzh) and viscous (Lyp and Lzp) terms:

hyperbolic operator: $Lyh(0-y_f,\ 0-z_h)$

$Lzh(0-y_h,\ 0-z_f)$

parabolic operator: $Lyp(0-y_f,\ 0-z_h)$

$Lzp(0-y_h,\ 0-z_f)$

With this further splitting, the stable time steps for the inner fine mesh and outer coarse mesh are about the same. The complete numerical procedure now is expressed as

$$U^{t+2\Delta t} = (LyLyhLyp)\cdot(LzLzhLzp)\cdot(Lx\cdot Lx)$$
$$\cdot(LzLzpLzh)\cdot(LyLypLyh)\,U^t$$

by which the solution is advanced two time steps from t to $t+2\Delta t$. Details of the numerical procedures and boundary conditions are described in Refs. 12 and 13.

Turbulence Model

Turbulence modeling for the three-dimensional configuration of Fig. 1 is complicated and not well developed. As $y\to\infty$, turbulence is dominated by the flat-plate surface $z=0$, and, on the other hand, as $z\to\infty$, turbulence is under the influence of wedge surface, $y=0$. In the axial corner region, turbulence is completely three-dimensional.

A turbulence model is developed based on the model of Escudier[16]:

$$\epsilon=\rho(D\ell)^2\omega \tag{1}$$

where D is the Van Driest damping factor:

$$D=1-\exp(-d\sqrt{|\tau_w|\rho_w}/26\mu_w) \tag{2}$$

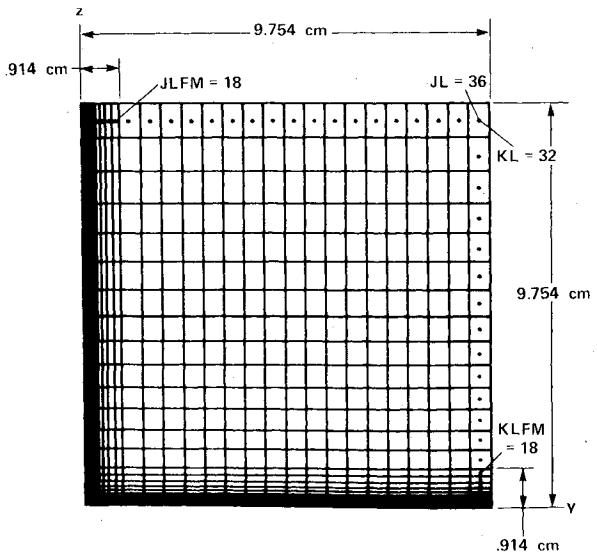

Fig. 5 Details of the mesh cells in (y-z) plane and the computational domain.

ω is absolute magnitude of vorticity:

$$\omega=|\nabla\times V|=\left[\left(\frac{\partial w}{\partial y}-\frac{\partial v}{\partial z}\right)^2+\left(\frac{\partial u}{\partial z}-\frac{\partial w}{\partial x}\right)^2+\left(\frac{\partial v}{\partial x}-\frac{\partial u}{\partial y}\right)^2\right]^{1/2} \tag{3}$$

ℓ is a mixing length scale:

$$\ell=\lambda\delta\tanh(0.41d/\lambda\delta) \tag{4}$$

and d is a "modified distance":

$$d=2yz/[(y+z)+\sqrt{y^2+z^2}] \tag{5}$$

Here δ is the value of d at the edge of the boundary layer, λ is a constant, and τ_w, ρ_w, μ_w are the values of shear stress, density, and molecular viscosity on the wall, respectively. In the present model, the viscous region in (y-z) plane is divided into four regions, I, II, III, IV, as shown in Fig. 3. In regions I and II, τ_w, ρ_w, and μ_w are evaluated at the wall $y=0$, and in regions III and IV, they are evaluated at the wall $z=0$. The edge of the boundary layer is located where the change of total velocity, $\Delta(u^2+v^2+w^2)/(u^2+v^2+w^2)$, is less than or equal to 2%, searching outward from the wall, either $y=0$ or $z=0$. The value of δ in regions II and III is treated as a constant, equal to the value of d at M, the intersection of 45 deg line and the edge of boundary layer. If the boundary-layer thicknesses on the two walls are substantially different, then the 45 deg line has to be modified. For the present calculation, the two thicknesses are nearly equal.

Equation (4) has been used previously (e.g., Ref. 17). It allows the length scale ℓ to change smoothly from $\ell\approx 0.41\,d$ as $d\to 0$ in the inner region to $\ell\to\lambda\delta$ as $d\to\infty$ in the outer region. The constaht λ is, in general, chosen between 0.10 and 0.07, depending on the type of flow. In the present study, $\lambda=0.08$. In Eq. (1), instead of the normal velocity gradient, the magnitude of vorticity ω is used. It is invariant with respect to the coordinate system and thus avoids the complication of corner regions. Note that, as $z\to\infty$,

$$\epsilon\approx\rho(D\ell)^2\left[\left(\frac{\partial u}{\partial y}\right)^2+\left(\frac{\partial w}{\partial y}\right)^2\right]^{1/2}$$

There is a similar formula for the outer region of y. The "modified distance" d results from a generalized formula of

$$1/d = \tfrac{1}{2}\int d\theta/s$$

integrating from $z=\infty$ to $z=0$ and then from $y=0$ to $y=\infty$ (Fig. 4). This integration formula can be applied to an arbitrary corner angle between the y and z planes. The use of the modified distance d is to account for the size of turbulence eddy or the turublence mixing length near the axial corner under the influence of both the y and z walls. In the special case of a two-dimensional flat plate, d is equal to the normal distance from the plate. Note that, as $z/y \to \infty$, $d \to y$, and $y/z \to \infty$, $d \to z$.

Results and Discussion

A swept shock wave generated from the leading edge of the wedge interacts with a turbulent boundary layer on the flat surface as shown in Fig. 1. The turbulent boundary layer is assumed fully developed at location $x=x_0$. Of main interest to this study is the interaction of the swept shock wave with the sidewall turbulent boundary layer. The experiments selected for comparison were conducted by Law,[15] and measurements were made of surface pressure and heat transfer on the flat surface ($z=0$). The flow conditions are given as follows: $M_\infty = 5.9$, $Re_L = 0.7083 \times 10^7$, $\alpha = 6$ and 12 deg, $T_\infty = 76.7$ K, $L = 21.6$ cm, and $T_w = 297.2$ K. The wall is treated as isothermal. A two-dimensional flat-plate calculation[18] is used to generate the upstream boundary conditions at $x_0/L = 0.868$, and then the three-dimensional flowfield is solved thereafter, down to $x/L = 1.921$, with equally spaced mesh points in the x direction. In the (y-z) plane, a total of (36×32) mesh points are used; the details of the mesh system and computational domain are shown in Fig. 5. For the geometrically stretched fine mesh, 18 mesh points are used in both y and z directions, with the minimum mesh spacing $\Delta y)_{\min} = \Delta z)_{\min} = (2L)/(3\sqrt{Re_L})$ and $y_f = z_f = 0.914$ cm. For the coarse mesh, 18 equally spaced mesh points are used in the y direction, and 14 geometrically stretched mesh points are used in the z direction, with $y_h = z_h = 9.754$ cm.

In the case of the present study, the Reynolds number is high, the boundary layer is thin, and the interaction feature is dominated strongly by the inviscid wedge shock, which grows linearly from the leading edge of the wedge. As a result, the flowfield is nearly conical downstream of the immediate vicinity of the leading-edge region. Figures 6 and 7 show comparisons of the present computed results with experimental measurements for surface pressure and heat transfer on the flat surface for two different wedge angles, $\alpha = 6$ and 12 deg. The distance is nondimensionalized with the shock distance y_s. The experimental data were obtained at $x/L = 1.53$ and 1.76, and show that the surface properties are essentially conical. The present numerical results are obtained at $x/L = 1.763$. The evaluation of the heat-transfer distribution is based on the gradient of total temperature T_t.

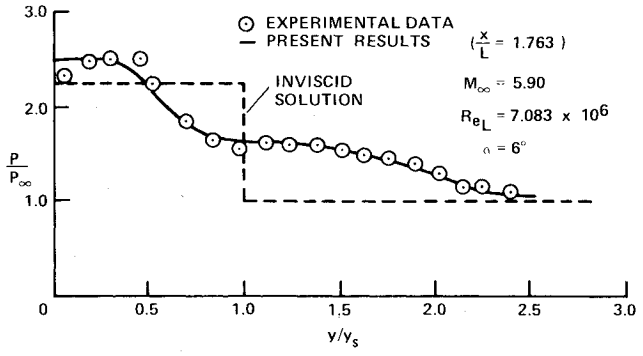

a) Surface pressure distribution

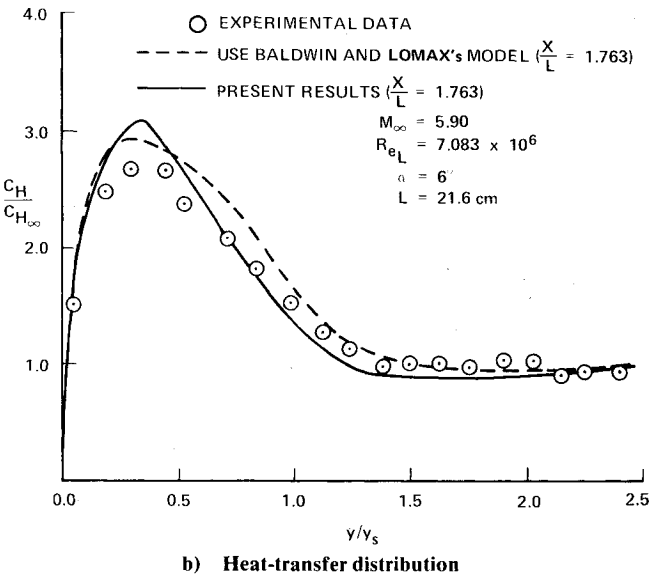

b) Heat-transfer distribution

Fig. 6 Comparison of surface pressure and heat transfer for $\alpha = 6$ deg.

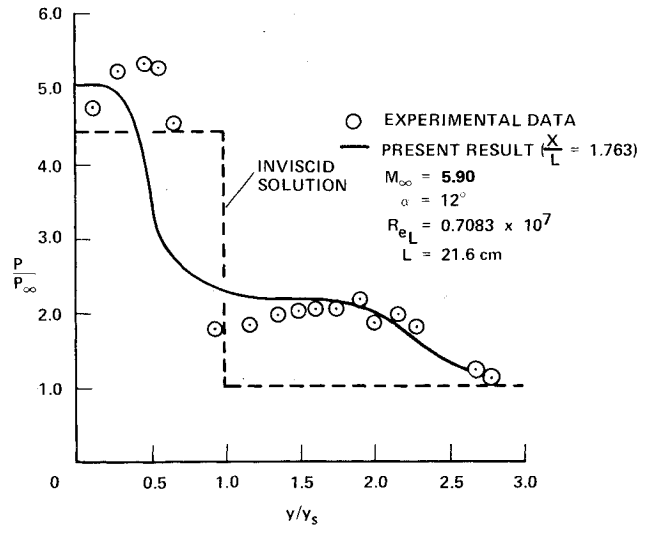

a) Surface pressure

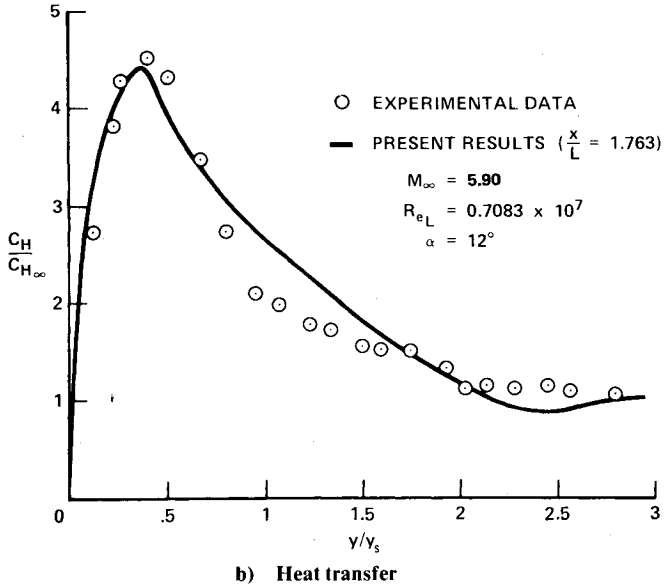

b) Heat transfer

Fig. 7 Comparison of computed and measured surface pressure; $\alpha = 12$ deg.

Through a simplified velocity and temperature relation

$$T_t \approx T + \frac{u^2}{2c_p} = T_w\left(1 - \frac{u}{u_\infty}\right) + T_\infty\left(1 + \frac{\gamma - 1}{2} M_\infty^2\right)\frac{u}{u_\infty}$$

it is noted that the gradients of static temperature T and total temperature T_t are identical at the wall where velocity vanishes. However, if u/u_∞ is linear near the wall, then T_t also is linear, while T is varying with an additional quadratic term.

Surprisingly enough, with such a simple eddy viscosity model for so complicated a three-dimensional interaction flow, the agreement is very good for the case of $\alpha = 6$ deg. For the case of $\alpha = 12$ deg, the computed results fail to show the existence of peak pressure found experimentally near the axial corner, and the location of the strong pressure gradient also is underpredicted. However, the range of interaction, the plateau pressure, and the value and location of peak heat transfer are predicted closely.

A two-layer eddy viscosity model, developed by Baldwin and Lomax,[14] has shown improvement over the model of Cebeci et al.[19] (Details of the model and the tested results are discussed in Ref. 14.) The model also has been extended in several publications.[20,21] In the present study, the "modified distance" d instead of normal distance is used, and the model is tested for the case of $\alpha = 6$ deg. The two models agree very well in surface pressure (not shown in the figure). The predicted heat transfer using Baldwin and Lomax's model also is included in Fig. 6b. The results using the two models agree reasonably well near the axial corner, $y/y_s < 0.25$, and the outer portion, $y/y_s > 2.0$. This is because the boundary layer is thick enough so that the heat-transfer rate is dominated by the inner eddy viscosity, which is similar for the two models. The deviation in peak heat transfer near

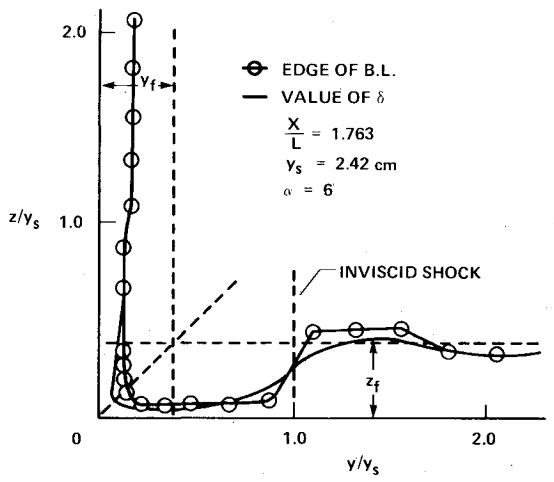

Fig. 8 Edge of boundary layer and the value of δ in $(y-z)$ plane.

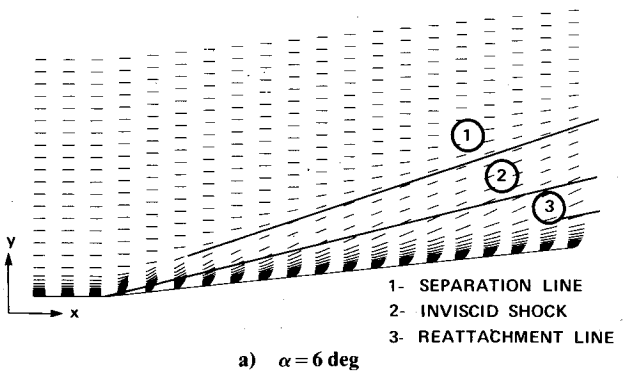

a) $\alpha = 6$ deg

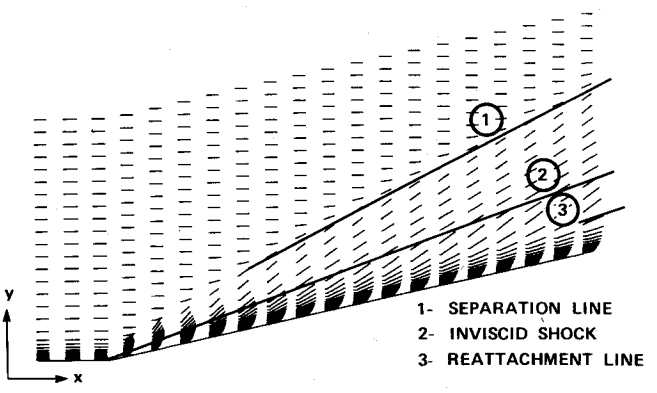

b) $\alpha = 12$ deg

Fig. 9 Velocity vector plots on surface, one mesh point above the wall $z = 0$.

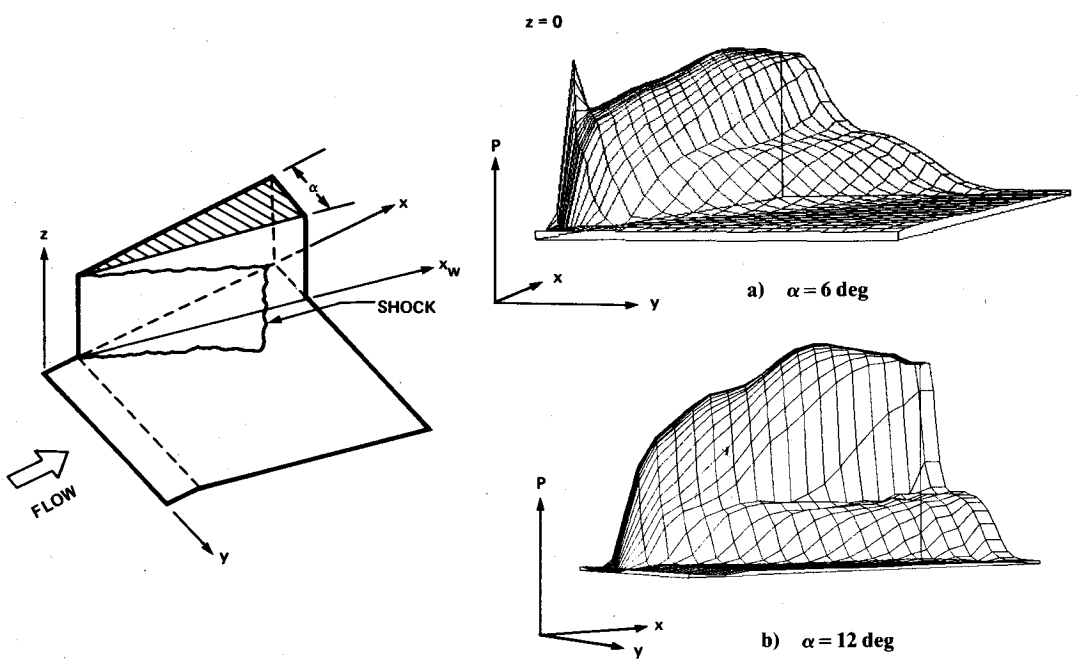

Fig. 10 Pressure on the wall $z = 0$.

$y/y_s = 0.5$ is because the boundary layer is very thin (discussed later), and not only the inner eddy viscosity but also the outer eddy viscosity, different in the two models, is needed to calculate heat transfer. Overall, these two models show about the same degree of agreement with the experimental measurements, and at the this time it is difficult to choose one over the other. Hereafter only the results using the model discussed in the previous section will be presented.

Figure 8 shows the boundary-layer thickness and the corresponding value of δ used in the computation in a (y-z) plane at $x/L = 1.763$ for $\alpha = 6$ deg. (Due to the application of a simple smoothing routine used in the calculation, δ may become slightly larger than the thickness of the boundary layer in regions of sharp change in boundary-layer thickness.) The location of the edge of the boundary layer shown in Fig. 8 confirms the earlier observation in Ref. 12 for the laminar case. High pressure behind the wedge shock compresses the boundary layer into a very thin layer and also pushes fluid outward in the y direction, causing a local bulge in the flat-plate boundary layer. This process scavenges off the low-momentum flow and brings fresh high-momentum flow into the inner axial corner region and, hence, causes high peak heat transfer. The sharp decrease of heat transfer is then caused by the pressure decreasing and the boundary-layer thickening in the outer region.

Figures 9a and 9b show the plots of velocity in the plane located just one mesh point above the wall ($z = 0$) for $\alpha = 6$ and 12 deg. (To keep the velocities in scale on a linear plot, the square root of velocity magnitude is used.) Due to thinning of the boundary layer, as discussed previously, the velocity in the inner corner region can be substantially larger than that in the outer region. For the case of $\alpha = 12$ deg, there clearly appears a line of velocity convergence which is, in general, interpreted

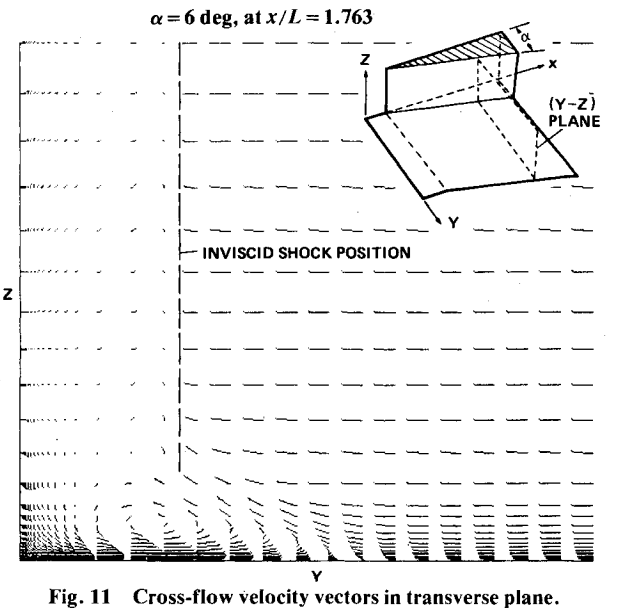

Fig. 11 Cross-flow velocity vectors in transverse plane.

as the line of separation. There is also a line, somewhat less clearly discernible, of velocity divergence in the inner region, very close to the maximum of the plotted velocity, which is due to strong pressure decrease and is, in general, interpreted as the line of reattachment. Indeed, these two lines of the present results agree very well with those of the experimental observation.

The three-dimensional plots of surface pressure on the complete surface of sidewall ($z = 0$) are shown in Figs. 10a and

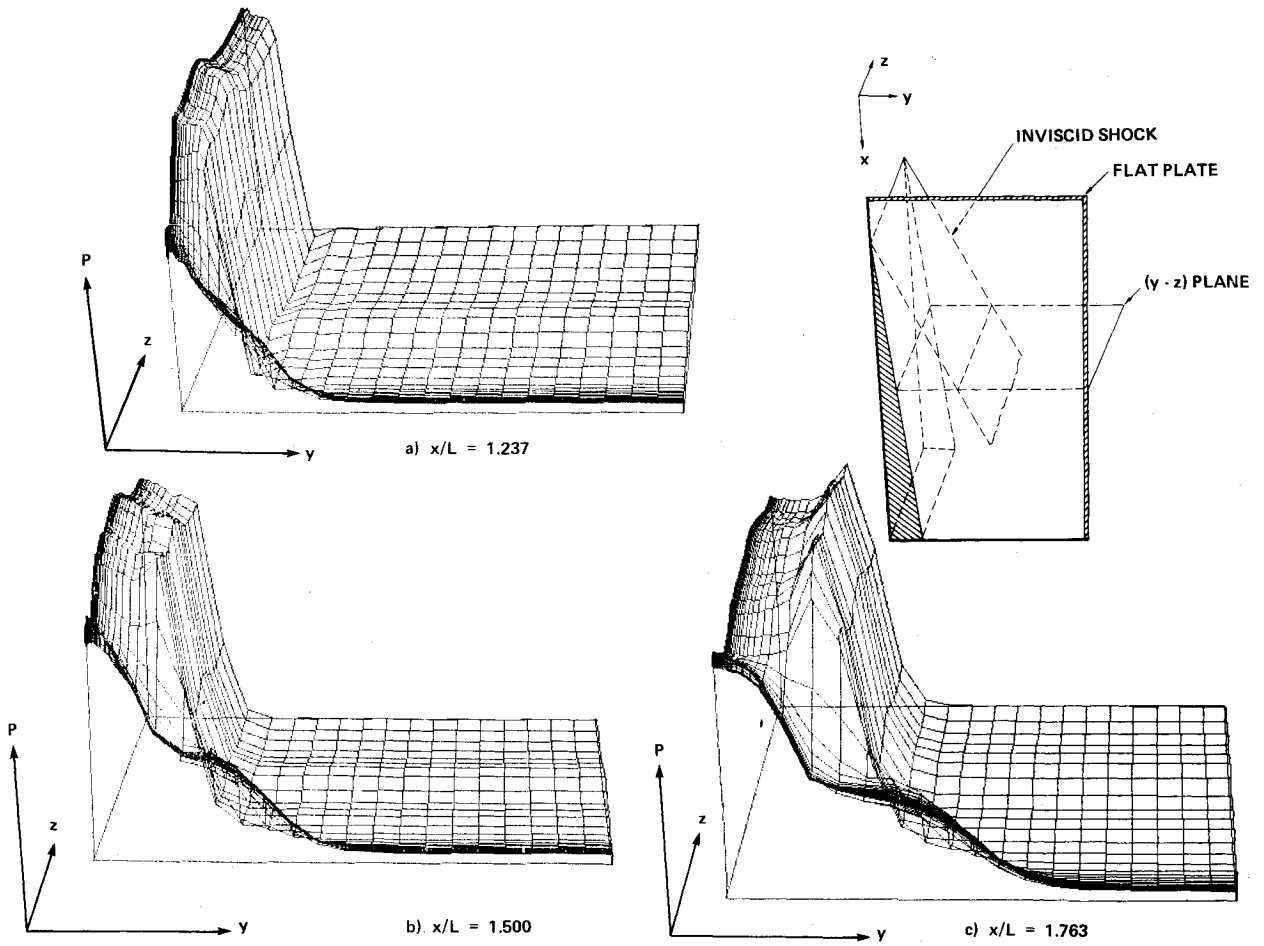

Fig. 12 Static pressure in the (y-z) planes at three streamwise stations.

10b for two different wedge angles. (The lines connect the values of surface pressure at each mesh point.) The surface pressure is shown to be nearly conical downstream of the vicinity of the leading edge, especially for the case of $\alpha = 6$ deg. Far downstream, one may expect that the flow will finally approach a quasi-two-dimensional solution. In Ref. 3, it was estimated, for that case, that it took a minimum distance of about 200 boundary-layer displacement thicknesses to reach a quasi-two-dimensional state. For the present case, the calculation extended approximately 60 boundary-layer displacement thicknesses.

In contrast to the sharp discontinuous wedge shock for $z \gg 0$ to be shown, the high pressure produced by the shock on or near the surface of $z = 0$ diffuses over a large range by interacting with the boundary layer. In the present calculation, the diffusion starts at about 0.4 of the shock distance y_s and extends over a range of about 2.5 times that distance, depending on wedge angle (Figs. 6 and 7a). For the case of $\alpha = 6$ deg, the total pressure rise is small. As the wedge angle increases to 12 deg, the pressure rise is substantially larger, and it is interesting to note the existence of a well-developed pressure plateau region between two sharp pressure rises, one large and one small, around the reattachment and separation lines. Near reattachment, the boundary layer is very thin and can sustain a strong pressure rise without extending it over a large area. However, the strong pressure gradient does force fluid in the boundary layer outward into the plateau region. The mechanism to damp out the induced cross-flow momentum in the y direction is very weak, and, finally, the outward flow peels off and results in a three-dimensional free shear layer separation. Figure 11 shows a cross-flow velocity plot, $v\cos\alpha - u\sin\alpha$ vs w, in a (y-z) plane. The existence of a vortex associated with the free shear layer separation is evident.

Figure 12 shows a sequence of static pressure plots in (y-z) planes at three-locations. As x increases, the wedge shock grows, and the range of interaction also increases. The wedge shock is well formed in the outer region. As it approaches the wall, the diffusion of pressure force in the boundary layer is observed clearly.

Calculation for the present $21 \times 36 \times 32$ meshes takes about 1.3 h of computation time on a CDC 7600 for a converged solution. This demonstrates, on comparison with our earlier results for laminar flow at a lower Reynolds number, that the computation time for the employed numerical scheme is nearly independent of Reynolds number.

Concluding Remarks

Supersonic turbulent flows over a three-dimensional corner have been simulated numerically. The complete mass-averaged Navier-Stokes equations with a simple eddy viscosity model are solved by a rapid numerical scheme. The three-dimensional interaction of the swept shock wave and turbulent boundary layer is studied. The high pressure near the flat surface of $z = 0$, generated by the swept shock, diffuses over a large range through boundary-layer interaction. As shock strength increases, the existence of a pressure plateau is shown clearly between two sharp pressure rises, a strong one near reattachment and a weak one near separation. The computed results do not show the existence of a peak surface pressure. The high peak heat-transfer rate is caused by the thinning of boundary layer and the incoming of fresh high-momentum and high-energy flow. The heat transfer then is relieved through the boundary-layer thickening in the outer region.

This is a preliminary investigation of a complex three-dimensional turbulent flowfield. Further study is needed to understand the details of inviscid-viscous interaction features. The problem of three-dimensional separation, which is quite different from the two-dimensional phenomenon, is still an unanswered question in the present study. Three-dimensional turbulence modeling is definitely a key issue for further numerical simulation.

References

[1] Stalker, R. J., "Sweepback Effects in Turbulent Boundary-Layer Interaction," *Journal of the Aerospace Sciences*, Vol. 27, May 1960, pp. 348-356.

[2] Stanbrook, A., "An Experimental Study of the Glancing Interaction between a Shock Wave and a Turbulent Boundary Layer," Aeronautical Research Council, ARC-CP-555, 1960.

[3] McCabe, A., "The Three-Dimensional Interaction of a Shock Wave with a Turbulent Boundary Layer," *Aeronautical Quarterly*, Vol. 17, Aug. 1966, pp. 231-252.

[4] Osham, B., Vas, I. E., and Bogdonoff, S. M., "An Experimental Study of Three-Dimensional Flow Field in an Axial Corner at Mach 3," AIAA Paper 77-689, Albuquerque, N. Mex., June 1977.

[5] Peake, D. T. and Rainbird, W. J., "The Three-Dimensional Separation of a Turbulent Boundary Layer by a Skewed Shock Wave; and Its Control by the Use of Tangential Air Injection," AGARD CP-168, Paper 40, May 1975.

[6] Neumann, R. D., "Recent Notes and Data on Interference Heating," Air Force Flight Dynamics Lab., AFFDL-TR-72-12, 1972.

[7] Kutler, P., "Numerical Solution for the Inviscid Supersonic Flow in the Corner Formed by Two Intersecting Wedges," AIAA Paper 73-675, Palm Springs, Calif., July 1973.

[8] Shankar, V., Anderson, D., and Kutler, P., "Numerical Solutions for Supersonic Corner Flow," *Journal of Computational Physics*, Vol. 17, July 1975, pp. 160-180.

[9] Shang, J. S. and Hankey, W. L., "Numerical Solution of the Navier-Stokes Equations for a Three-Dimensional Corner," *AIAA Journal*, Vol. 15, Nov. 1977, pp. 1575-1582.

[10] MacCormack, R. W. and Baldwin, B. S., "A Numerical Method for Solving the Navier-Stokes Equations with Application to Shock-Boundary Layer Interactions," AIAA Paper 75-1, Pasadena, Calif., Jan. 1975.

[11] Shang, J. S., "An Implicit-Explicit Method for Solving the Navier-Stokes Equations," *AIAA Journal*, Vol. 16, May 1978, pp. 496-502.

[12] Hung, C. M. and MacCormack, R. W., "Numerical Solution of Supersonic Laminar Flow over a Three-Dimensional Compression Corner," AIAA Paper 77-694, Albuquerque, N. Mex., June 1977.

[13] MacCormack, R. W., "An Efficient Numerical Method for Solving the Time-Dependent Compressible Navier-Stokes Equations at High Reynolds Number," NASA TM X-73,129, July 1976.

[14] Baldwin, B. S. and Lomax, H., "Thin Layer Approximation and Algebraic Model for Separated Turbulent Flows," AIAA Paper 78-257, Huntsville, Ala., Jan. 1978.

[15] Law, C. H., "Three-Dimensional Shock Wave—Turbulent Boundary Layer Interactions at Mach 6," Aerospace Research Labs., Wright-Patterson Air Force Base, Ohio, ARL TR 75-0191, June 1975.

[16] Escudier, M. P., "The Distribution of the Mixing Length in Turbulent Flows Near Walls," Imperial College, Mechanical Engineering Dept., London, Rept. TWF/TN/1, 1965.

[17] McDonald, H. and Camarata, F. J., "An Extended Mixing Length Approach for Computing the Turbulent Boundary Layer Development," *Proceedings of Computation of Turbulent Boundary Layer—1968 AFOSR-IFP-Stanford Conference*, Vol. I, Aug. 1968, pp. 83-98.

[18] Hung, C. M. and MacCormack, R. W., "Numerical Simulation of Supersonic and Hypersonic Turbulent Compression Corner Flows," *AIAA Journal*, Vol. 15, March 1977, pp. 410-416.

[19] Cebeci, T., Smith, A. M. O., and Mosinskis, G., "Calculations of Compressible Adiabatic Turbulent Boundary Layer," *AIAA Journal*, Vol. 8, Nov. 1970, pp. 1974-1982.

[20] Steger, J. I., "Implicit Finite Difference Simulation of Flow About Arbitrary Two-Dimensional Geometries," *AIAA Journal*, Vol. 16, July 1978, pp. 679-686.

[21] Pulliam, T. H. and Steger, J. S., "On Implicit Finite Difference Simulations of Three-Dimensional Flow," AIAA Paper 78-10, Huntsville, Ala., Jan. 1978.